International Journal of Applied Engineering and Technology ISSN: 2277-212X (Online)
An Online International Journal Available at http://www.cibtech.org/jet.htm
2012 Vol. 2 (1) January-March, pp12-22/Upadhyay and Shanker
Research Article

VISCOUS INCOMPRESSIBLE FLUID FLOW THROUGH A CURVED CHANNEL WITH DIFFERENTIALLY HEATED VERTICAL SIDEWALLS

***Rabindra Nath Mondal[1], Md. Kutub Uddin[2] and Md. Rezaul Karim[3]**
**Mathematics Discipline, Khulna University, Khulna-9208, Bangladesh.*
Dept. of Mathematics, University of Dhaka, Dhaka-1000, Bangladesh
Dept. of Mathematics, Jagannath University, Dhaka-1204, Bangladesh
**Author for Correspondence*

ABSTRACT
In this paper, a numerical study is presented for the non-isothermal flows through a curved rectangular duct of aspect ratios ranging from 1 to 4 at a constant curvature 0.1. Numerical calculations are carried out by using a spectral method for the Dean number *Dn* = 100 with a temperature difference between the vertical sidewalls for the Grashof numbers, *Gr* = 100, 500 and 1000, where the outer wall is heated and the inner wall cooled. The main concern of the present study is to investigate the unsteady flow characteristics through a curved rectangular duct as the aspect ratio is increased. With a view to study the non-linear behavior of the unsteady solutions, time evolution calculations of the unsteady solutions are obtained, and it is found that the steady-state solution turns into time periodic solution if the Dean number or the Grashof number is increased. For large aspect ratios, it is found that the chaotic solutions appear at small *Dn* or *Gr*. Effect of secondary vortices on unsteady solutions are also investigated.

Key Words*: Curved Duct; Non-Isothermal Flows; Steady Solutions; Dean Number; Grashof Number*

INTRODUCTION
The study of flows through a curved duct is of fundamental interest because of its ample applications in fluids engineering, such as in air conditioning systems, refrigeration, heat exchangers, ventilators, and the blade-to-blade passages in modern gas turbines. Blood flow in human veins and arteries is another important application of the curved duct flows. The flow through a curved duct shows physically interesting feature under the action of the centrifugal force caused by the curvature of the duct. The presence of curvature generates centrifugal forces which act at right angle to the main flow direction and produce secondary flows. Dean (1927) was the first who formulated the problem in mathematical terms under the fully developed flow condition. He found the secondary flow consisting of a pair of counter rotating vortices caused by the centrifugal force. Since then, there have been a lot of theoretical and experimental works concerning this flow. Berger *et al.* (1983), Nandakumar and Masliyah (1986) and Ito (1987) may be referred to for some outstanding reviews on curved duct flows.
One of the interesting phenomena of the flow through a curved duct is the bifurcation of the flow because generally there exist many steady solutions due to channel curvature. Dennis and Ng (1982) and Nandakumar and Masliyah (1982) studied dual solutions of the flow through a curved duct. Yang and Keller (1986) studied the bifurcation of the flow for small curvature and found multiple branches of solutions. An early bifurcation structure and linear stability of the steady solutions for fully developed flows in a curved square duct was investigated by Winters (1987). He applied bifurcation analysis to it and found that there are many symmetric and asymmetric steady solutions among which linearly stable ones are few. However, the existence of the multiple solutions of the flow through a curved duct with the large aspect ratio was first studied by Yanase and Nishiyama (1988). They obtained two kinds of solutions: the two-vortex solution and the four-vortex solution for the same aspect ratio. Wang and Yang (2004) performed a numerical study on fully developed bifurcation structure and stability of the forced convection in a curved square duct flow. Recently, Mondal *et al*. (2006) performed numerical prediction of non-isothermal flows through a curved square duct with the effects of curvature. Very recently,

Mondal *et al*. (2010) performed numerical prediction of secondary flow and unsteady solutions through a curved rectangular duct of aspect ratio and revealed some new features of unsteady flow behavior through a curved channel.

One of the most important applications of curved duct flow is to enhance the thermal exchange between two sidewalls, because it is possible that the secondary flow may convey heat and then increases heat flux between two sidewalls. Chandratilleke and Nursubyakto (2003) presented numerical calculations to describe the secondary flow characteristics in the flow through curved ducts of aspect ratios ranging from 1 to 8 that were heated on the outer wall, where they studied for small Dean numbers and compared the numerical results with their experimental data. Recently, Yanase *et al*. (2005a) performed numerical investigation of thermal (Gr = 100) and non-thermal flows (Gr = 0) through a curved rectangular duct with differentially heated vertical sidewalls, where they obtained many branches of steady solutions and addressed the time-dependent behavior of the unsteady solutions. In the succeeding paper, Yanase *et al*. (2005b) studied the bifurcation structure as well as the effects of secondary flows on convective heat transfer for moderate Grashof numbers. However, complete bifurcation structure as well as transient behavior of the unsteady solutions for the Dean approximation are yet unresolved, which is important from both engineering and scientific point of view.

In the present paper, numerical results are presented for the fully developed two-dimensional flow of viscous incompressible fluid through a curved duct with differentially heated vertical sidewalls for various aspect ratios. The aim of the paper is to investigate the flow characteristics with the investigation of time-dependent behavior of the unsteady solutions.

2. Basic Equations

Consider a hydrodynamically and thermally fully developed two-dimensional flow of viscous incompressible fluid through a curved duct with a constant curvature. The cross section of the duct is a rectangle with width $2d$ and height $2h$. It is assumed that the outer wall of the duct is heated while the inner one is cooled. The temperature of the outer wall is $T_0 + \Delta T$ and that of the inner wall is $T_0 - \Delta T$, where $\Delta T > 0$. The x, y and z axes are taken to be in the horizontal, vertical, and axial directions, respectively. It is assumed that the flow is uniform in the axial direction (i.e. in the z direction), and that it is driven by a constant pressure gradient G along the center-line of the duct, that is, the main flow in the axial direction as shown in Fig. 1.

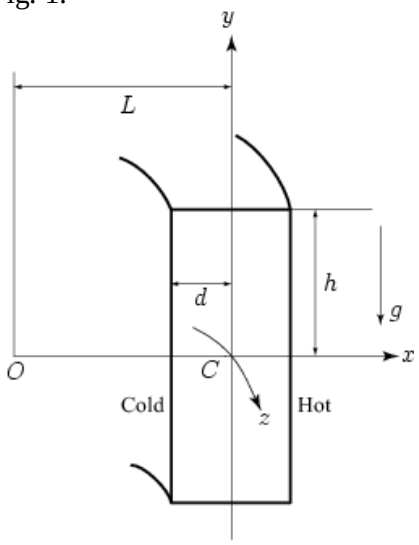

Figure 1: Coordinate system of the curved rectangular duct.

The variables are non-dimensionalized by using of the representative length *d*, the representative velocity $U_0 = \nu / d$, where ν is the kinematic viscosity of the fluid. We introduce the non-dimensional variables defined as

$$u = \frac{u'}{U_0},\ v = \frac{v'}{U_0}, w = \frac{\sqrt{2\delta}}{U_0} w',\ x = \frac{x'}{d},\ \bar{y} = \frac{y'}{d},\ z = \frac{z'}{d}$$

$$T = \frac{T'}{\Delta T},\ t = \frac{U_0}{d} t',\ \delta = \frac{d}{L},\ P = \frac{P'}{\rho U_0^{\ 2}}$$

where u, v and w are the non-dimensional velocity components in the x, y and z directions, respectively; t is the non-dimensional time, P the non-dimensional pressure, δ the non-dimensional curvature defined as $\delta = \frac{d}{L}$, and temperature is non-dimensionalized by ΔT. In the above method of non-dimensionalization, the variables with prime denote the dimensional quantities. Since the flow field is uniform in the z-direction, the sectional stream function ψ is introduced as follows:

$$u = \frac{1}{1+\delta x}\frac{\partial \psi}{\partial y}, \quad v = -\frac{1}{1+\delta x}\frac{\partial \psi}{\partial x} \tag{2.1}$$

We introduce a new coordinate variable y in the $\bar{y}$-direction as $\bar{y} = ly$, where $l = h/d$ is the aspect ratio of the duct cross section. Then basic equations for w, ψ and *T* are derived from the Navier-Stokes equations and the heat-conduction equation with the Boussinesq approximation as follows:

$$(1+\partial x)\frac{\partial w}{\partial t} + \frac{1}{l}\frac{\partial(w,\psi)}{\partial(x,y)} - D_n + \frac{\delta^2}{(1+\delta x)} = (1+\delta x)\Delta_2 w - \frac{1}{l}\frac{\delta}{(1+\delta x)}\frac{\partial \psi}{\partial y} w + \delta \frac{\partial w}{\partial x}, \tag{2.2}$$

$$\left(\Delta_2 - \frac{\delta}{1+\delta x}\frac{\partial}{\partial x}\right)\frac{\partial \psi}{\partial t} = -\frac{1}{l}\frac{1}{1+\delta x}\frac{\partial(\Delta_2\psi,\psi)}{\partial(x,y)} + \frac{1}{l}\frac{\delta}{(1+\delta x)^2}$$
$$\times\left[\frac{\partial \psi}{\partial y}\left(2\Delta_2\psi - \frac{3\delta}{1+\delta x}\frac{\partial \psi}{\partial x} + \frac{\partial^2 \psi}{\partial x^2}\right) - \frac{\partial \psi}{\partial x}\frac{\partial^2 \psi}{\partial x \partial y}\right] + \frac{\delta}{(1+\delta x)^2}\left[3\delta\frac{\partial^2 \psi}{\partial x^2} - \frac{3\delta^2}{1+\delta x}\frac{\partial \psi}{\partial x}\right]$$
$$-\frac{2\delta}{(1+\delta x)}\frac{\partial}{\partial x}\Delta_2\psi + \frac{1}{l} w\frac{\partial w}{\partial y} + \Delta_2^2\psi - Gr(1+\delta x)\frac{\partial T}{\partial x}, \tag{2.3}$$

$$\frac{\partial T}{\partial t} + \frac{1}{l}\frac{1}{1+\delta x}\frac{\partial(\psi,T)}{\partial(x,y)} = \frac{1}{\mathrm{Pr}}\left(\Delta_2 T + \frac{\delta}{1+\delta x}\right), \tag{2.4}$$

where

$$\Delta_2 \equiv \frac{\partial^2}{\partial x^2} + \frac{1}{l^2}\frac{\partial^2}{\partial y^2}, \quad \frac{\partial(f,g)}{\partial(x,y)} \equiv \frac{\partial f}{\partial x}\frac{\partial g}{\partial y} - \frac{\partial f}{\partial y}\frac{\partial g}{\partial x}. \tag{2.5}$$

Dn, *Gr* and *Pr*, which appear in Eqs. (2.2) - (2.4) are defined as

$$Dn = \frac{Gd^3}{\mu\nu}\sqrt{\frac{2d}{L}}, \quad Gr = \frac{\gamma g \Delta T d^3}{\nu^2}, \quad Pr = \frac{\nu}{\kappa}. \tag{2.6}$$

where μ, γ, κ and g are the viscosity, the coefficient of thermal expansion, the coefficient of thermal diffusivity and the gravitational acceleration, respectively. G is the pressure gradient along the duct axis

and is taken to be positive. In the present study, *Gr* and *l* (aspect ratio) vary, while δ , *Dn* and *Pr* are fixed as $\delta = 0.1$, *Dn* = 100 and *Pr* = 7.0 (water).
The rigid boundary conditions for w and ψ are

$$w(\pm 1, y) = w(x, \pm 1) = \psi(\pm 1, y) = \psi(x, \pm 1) = \frac{\partial \psi}{\partial x}(\pm 1, y) = \frac{\partial \psi}{\partial y}(x, \pm 1) = 0, \qquad (2.7)$$

and the conducting boundary conditions for *T* are assumed as

$$T(1, y) = 1,\ T(-1, y) = -1,\ T(x, \pm 1) = x. \qquad (2.8)$$

3. Numerical Calculations

In order to solve the Eqs. (2.2) - (2.4) numerically, the spectral method is used. This is the method which is thought to be the best numerical method to solve the Navier-Stokes equations as well as the energy equation. Details of this method are discussed in Mondal (2006). By this method the variables are expanded in a series of functions consisting of the Chebyshev polynomials. That is, the expansion functions $\Phi_n(x)$ and $\Psi_n(x)$ are defined as

$$\Phi_n(x) = (1 - x^2) C_n(x),\ \Psi_n(x) = (1 - x^2)^2 C_n(x), \qquad (3.1)$$

where $C_n(x) = cos(n\, cos^{-1}(x))$ is the *n*-th order Chebyshev polynomial. $w(x, y, z)$, $\psi(x, y, t)$ and $T(x, y, t)$ are expanded in terms of $\Phi_n(x)$ and $\Psi_n(x)$ as

$$\left.\begin{aligned} w(x, y, z) &= \sum_{m=0}^{M} \sum_{n=0}^{N} w_{mn}(t) \Phi_m(x) \Phi_n(y), \\ \psi(x, y, t) &= \sum_{m=0}^{M} \sum_{n=0}^{N} \psi_{mn}(t) \Psi_m(x) \Psi_n(y), \\ T(x, y, t) &= \sum_{m=0}^{M} \sum_{n=0}^{N} T_{mn}(t) \Phi_m(x) \Phi_n(y) + x, \end{aligned}\right\} \qquad (3.2)$$

where M and N are the truncation numbers in the x- and y-directions, respectively. The expansion coefficients w_{mn} , ψ_{mn} and T_{mn} are then substituted into the basic Eqs. (2.2), (2.3) and (2.4) and the collocation method is applied. As a result, the nonlinear algebraic equations for w_{mn} , ψ_{mn} and T_{mn} are obtained. The collocation points are taken to be

$$\left.\begin{aligned} x_i &= cos\left[\pi\left(1 - \frac{i}{M+2}\right)\right], \qquad i = 1, \ldots, M+1 \\ y_j &= cos\left[\pi\left(1 - \frac{j}{N+2}\right)\right], \qquad j = 1, \ldots, N+1 \end{aligned}\right\}, \qquad (3.3)$$

The steady solutions are then obtained by the Newton-Raphson iteration method assuming that all the coefficients are time independent. Finally, in order to calculate the time-dependent solutions, the Crank-Nicolson and Adams-Bashforth methods together with the function expansion (3.2) and the collocation method are applied. We performed numerical calculations for *Gr* = 100, 500 and 1000 at *Dn* = 100 for the aspect ratios $l = 1, 2$, 3 and 4.

4. Resistance Coefficient

We use the resistance coefficient λ as one of the representative quantities of the flow state. It is also called the hydraulic resistance coefficient, and is generally used in fluids engineering, defined as

$$\frac{P_1^* - P_2^*}{\Delta z^*} = \frac{\lambda}{dh^*}\frac{1}{2}\rho\left\langle w^* \right\rangle^2, \tag{4.1}$$

where quantities with an asterisk denote dimensional ones, $\langle\ \rangle$ stands for the mean over the cross section of the rectangular duct, and $d_h^* = 4(2d \times 2dl)/(4d \times 4dl)$. The mean axial velocity $\langle w^* \rangle$ is calculated by

$$\langle w^* \rangle = \frac{\nu}{4\sqrt{2\delta}ld}\int_{-1}^{1} dx \int_{-1}^{1} \overline{w}(x, y)dy. \tag{4.2}$$

Since $(P_1^* - P_2^*)/\Delta z^* = G$, λ is related to the mean non-dimensional axial velocity $\langle w \rangle$ as

$$\lambda = \frac{8l\sqrt{2\delta}Dn}{(1+l)\langle w \rangle^2}, \tag{4.3}$$

where $\langle w \rangle = \sqrt{2\delta}d / \nu\langle w^* \rangle$.

In this paper, we use λ to discriminate steady solution branches and to pursue the time evolution of the unsteady solutions.

5. RESULTS AND DISCUSSION

In order to study the non-linear behavior of the unsteady solutions, time-evolution calculations of the resistance coefficient λ, given by Eq. (4.3), are performed. Numerical calculations are carried out for $\delta = 0.1$, $\mathrm{Pr} = 7.0$, $Dn = 100$ and $Gr = 100, 500$ and 1000 for the aspect ratios $l = 1, 2, 3$ and 4.

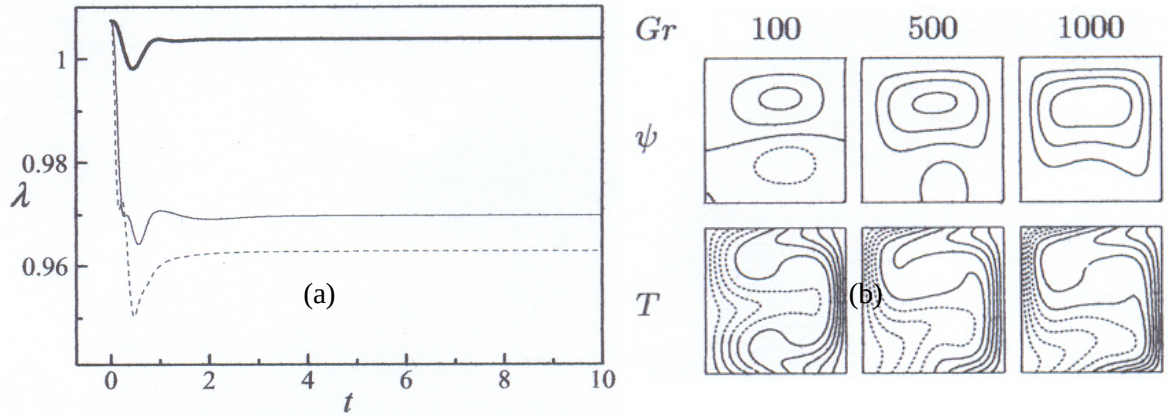

Figure 2: (a) Time-evolution of λ with the thermal effect for *Dn* = 100 and *l* = 1 (square duct) for *Gr* = 100, 500 and 1000 (thick solid line: *Gr* = 100, thin solid line: *Gr* = 500, dashed line: *Gr* = 1000). (b) Secondary flow patterns (top) and temperature distributions (bottom) for various values of *Gr* at *Dn* = 100 and *l* = 1 at time *t* = 10.

We perform time-evolution calculation of the resistance coefficient λ for *Dn* = 100 and $l = 1$ (square duct) as shown in Fig. 2(a). In this figure, a thick solid line stands for *Gr* = 100, a thin solid line *Gr* = 500, and a dashed line *Gr* = 1000. As seen in Fig. 2(a), the flow approaches a steady-state immediately for all three cases of *Gr*, and λ becomes small if *Gr* is increased. Since the unsteady flow is steady-state solution, a single contour of secondary flow pattern and the temperature profile is shown in Fig. 2(b) at time *t* = 10, where the contours of ψ and *T* are drawn with the increments $\Delta\psi$ = 0.8 and ΔT = 0.2, respectively. The same increments of ψ, and *T* are used for all the figures in this paper, if not specified. In the figures of the secondary flow, solid lines $(\psi \geq 0)$ show that the secondary flow is in the counter

clockwise direction while the dotted lines $(\psi < 0)$ in the clockwise direction. Similarly, in the figures of the temperature field, solid lines are those for $T \geq 0$ and dotted ones for $T < 0$. As seen in Fig. 2(b), the unsteady flow is a two-vortex solution for *Dn* = 100 and *Gr* = 100 and 500 for *l* = 1, but a single-vortex solution for *Dn* = 100 and *Gr* = 100 for *l* = 1. It is found that when *Gr* becomes large the symmetry with respect to $y = 0$ breaks. The reason is that the effect of buoyancy force becomes comparable as that of centrifugal force when the temperature difference becomes large. As seen in Fig. 2(b), the temperature profile is consistent with the secondary vortices, and the temperature is distributed significantly from the heated wall (outer wall) to the fluid as the Grashof number becomes high.

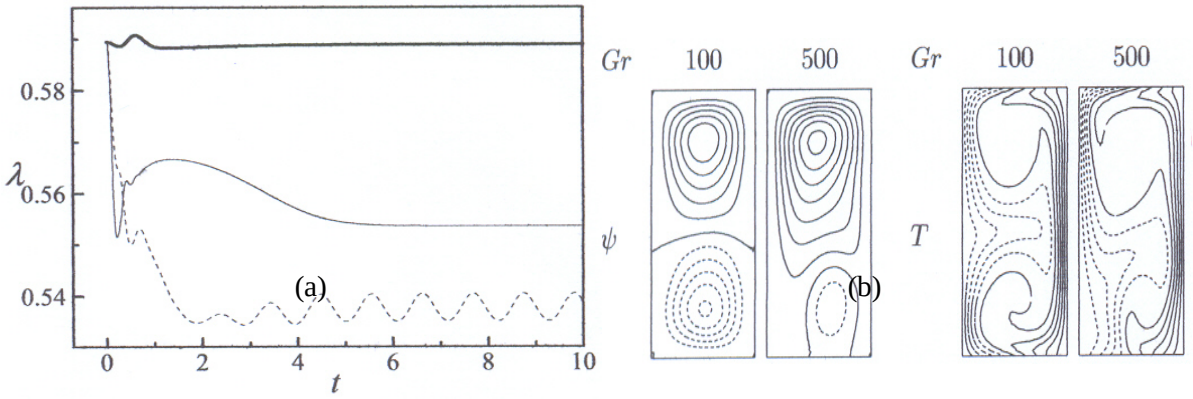

Figure 3: (a) Time-evolution of λ with the thermal effect for *Dn* = 100 and *l* = 2 for *Gr* = 100, 500 and 1000 (thick solid line: *Gr* = 100, thin solid line: *Gr* = 500, dashed line: *Gr* = 1000). (b) Secondary flow patterns and temperature distributions for *Gr* =100 and 500 at *Dn* = 100 and *l* = 2 at time *t* = 10.

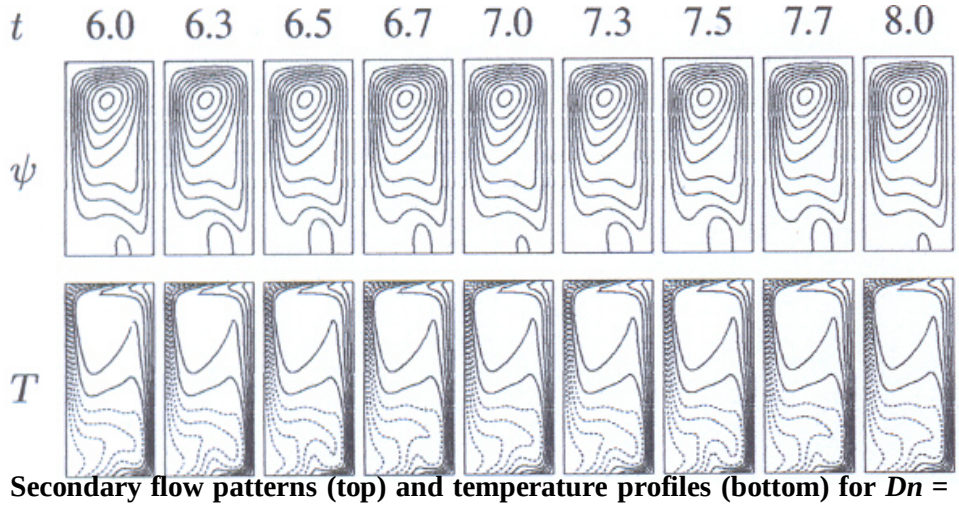

Figure 4: Secondary flow patterns (top) and temperature profiles (bottom) for *Dn* = 100, *l* = 2 and *Gr* = 1000 for one period of oscillation at time $6.0 \leq t \leq 8.0$.

Then we perform time-evolution calculation of λ for the aspect ratio *l* = 2 at *Dn* = 100 with the thermal effect at *Gr* = 100, 500 and 1000, as shown in Fig. 3(a). It is found that the unsteady flow attains a steady-state solution for *Gr* =100 and 500, but oscillates periodically for *Gr* = 1000. Since the flow is a steady-state solution for *Gr* =100 and 500 at *Dn* = 100, we show a single contour of secondary flow pattern and the temperature profile for *Gr* = 100, 500 in Fig. 3(b) at time *t* = 10. Figure 4 shows typical contours of secondary flow patterns and temperature profiles for the periodic oscillation at *Dn* = 100 and *Gr* = 1000 at *l* = 2, for one period of oscillation at time $6.0 \leq t \leq 8.0$. As seen in Fig. 4, the secondary flow is an

asymmetric two-vortex solution; one is a large vortex dominating the smaller one. The periodic change is clearly observed in the secondary flow patterns and in temperature distributions as seen in Fig. 4.

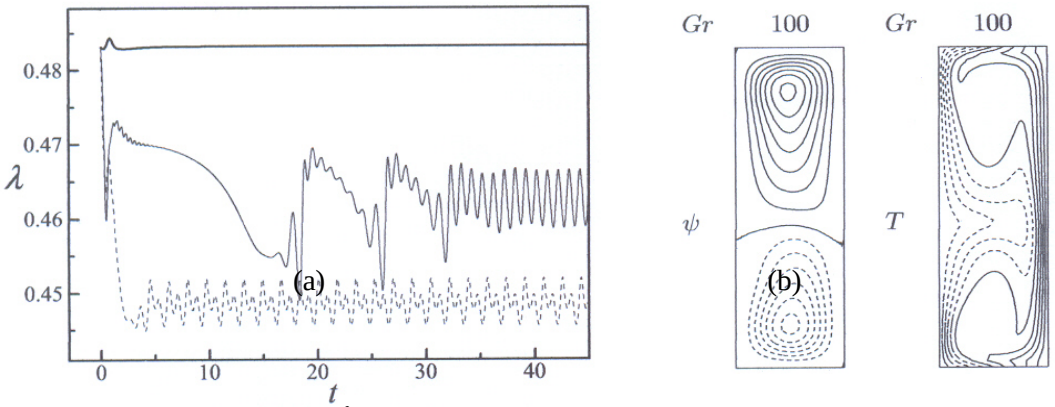

Figure 5: Time-evolution of λ with the thermal effect for *Dn* = 100 and *l* = 3 for *Gr* = 100, 500 and 1000. (thick solid line: *Gr* = 100, thin solid line: *Gr* = 500, dashed line: *Gr* = 1000). (b) Secondary flow pattern (left) and temperature profile (right) for *Dn* = 100, *l* = 3 and *Gr* = 100 at time *t* = 30.

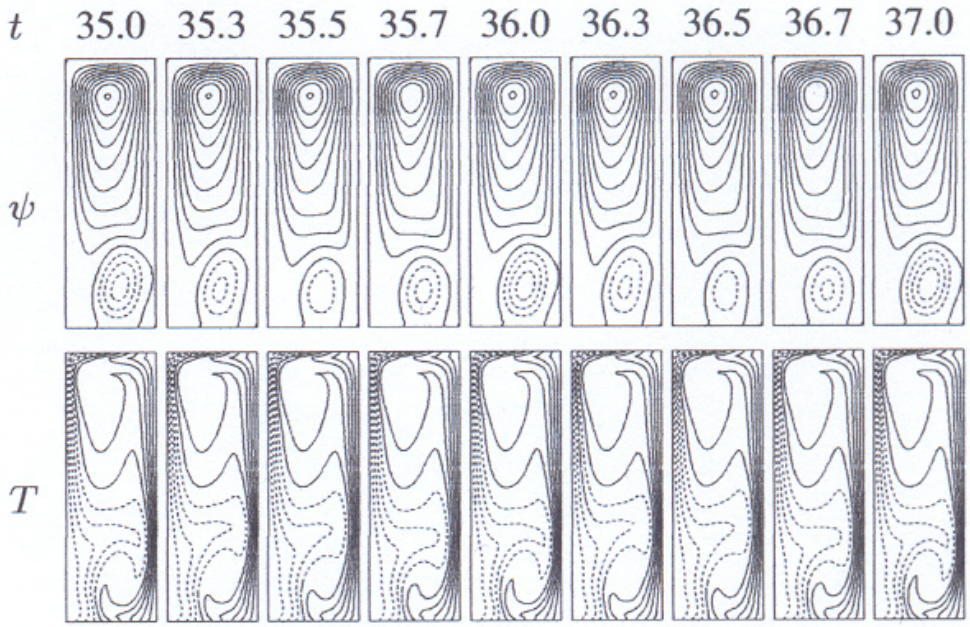

Figure 6: Secondary flow patterns and temperature distributions for *Dn* = 100, *Gr* = 500 for the aspect ratio *l* = 3 at time $35.0 \le t \le 37.0$ **.**

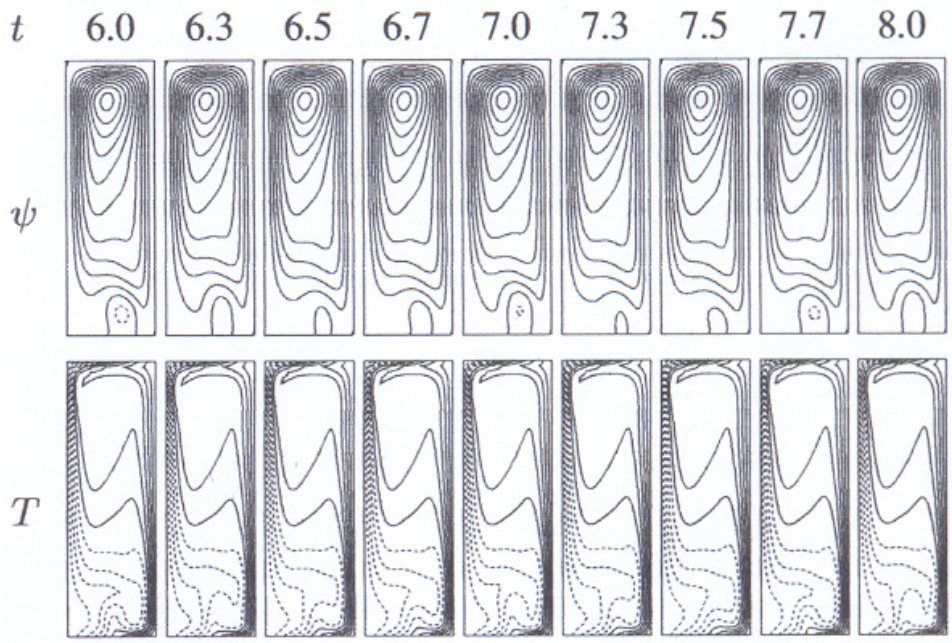

Figure 7: Secondary flow patterns and temperature distributions for *Dn* = 100, *Gr* = 1000 for the aspect ratio *l* = 3 at time $6.0 \le t \le 8.0$ **.**

We show the time-evolution of λ with the thermal effect for *Gr* = 100, 500 and 1000 and *Dn* = 100 for the aspect ratio *l* = 3 in Fig. 5(a). As seen in Fig. 5(a), the unsteady flow is a steady-state solution for *Gr* = 100 but a periodic solution at *Gr* = 500 and a periodic solution consisting with plural periods (i.e. multi-periodic solution) at *Gr* = 1000. Since the flow is a steady-state solution for *Gr* =100, *Dn* = 100 and *l* = 3, we show a single contour of secondary flow pattern and the temperature profile at time *t* = 30 in Fig. 5(b). It is found that the steady-state solution is an asymmetric two-vortex solution. In order to see the periodic change of the flow patterns, as time proceeds, typical contours of secondary flow patterns and temperature profiles for *Dn* = 100 and *Gr* = 500 at *l* = 3 are shown in Fig. 6 for one period of oscillation at time $35.0 \le t \le 37.0$. As seen in Fig. 6, the periodic oscillation at *Gr* = 500 is an asymmetric two-vortex solution. Then we show typical contours of secondary flow patterns and temperature distributions for the multi-periodic oscillation at *Dn* = 100, *Gr* = 1000 for the aspect ratio *l* = 3 in Fig. 7, for one period of oscillation at time $6.0 \le t \le 8.0$, where it is seen that the unsteady flow at *Gr* = 1000 oscillates periodically between the asymmetric two-vortex solutions with one large vortex dominating the smaller one. It is found that though the symmetry with respect to $y = 0$ is approximately maintained for *Gr* = 100 (see Fig. 5(b)), it completely disappears if *Gr* is increased more. In Figs. 6 and 7, the periodic oscillations of the time-dependent flows are observed. From these results, it is found that the oscillation tends to occur when the Grashof number or the aspect ratio is increased keeping the Dean number fixed. The temperature distribution is consistent with the secondary vortices, and convective heat transfer is observed from the heated wall to the fluid as the Grashof number is increased.

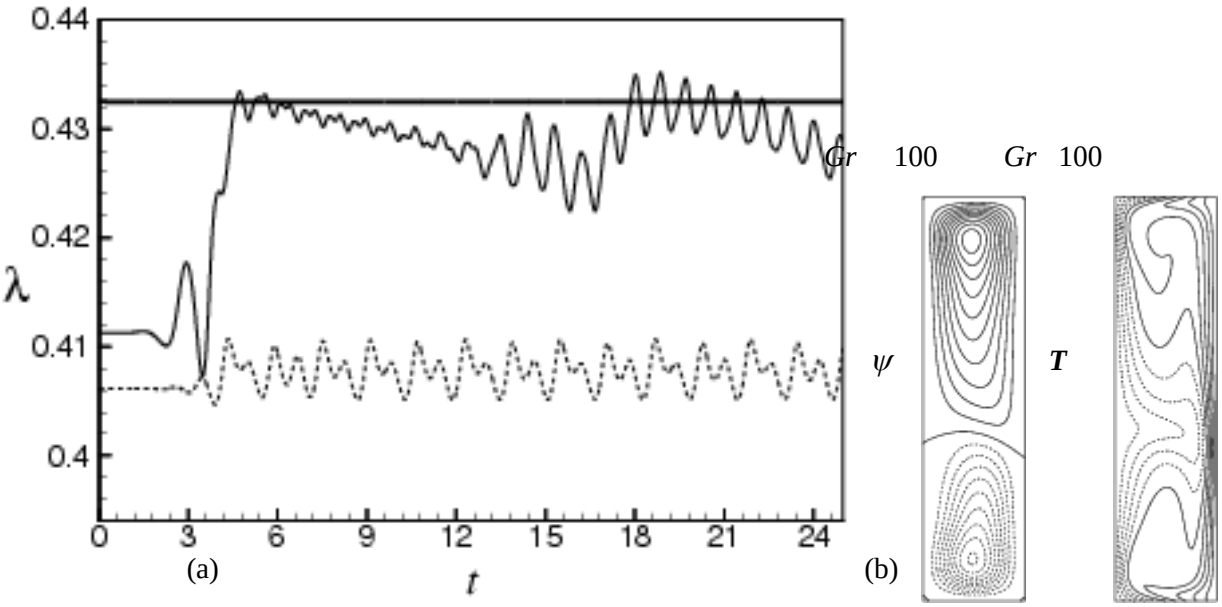

Figure 8: Time-evolution of λ with the thermal effect for *Dn* = 100 and *l* = 4 for *Gr* = 100, 500 and 1000. (thick solid line: *Gr* = 100, thin solid line: *Gr* = 500, dashed line: *Gr* = 1000). (b) Secondary flow pattern (left) and temperature profile (right) for *Dn* = 100, *l* = 4 and *Gr* = 100 at time *t* = 20.

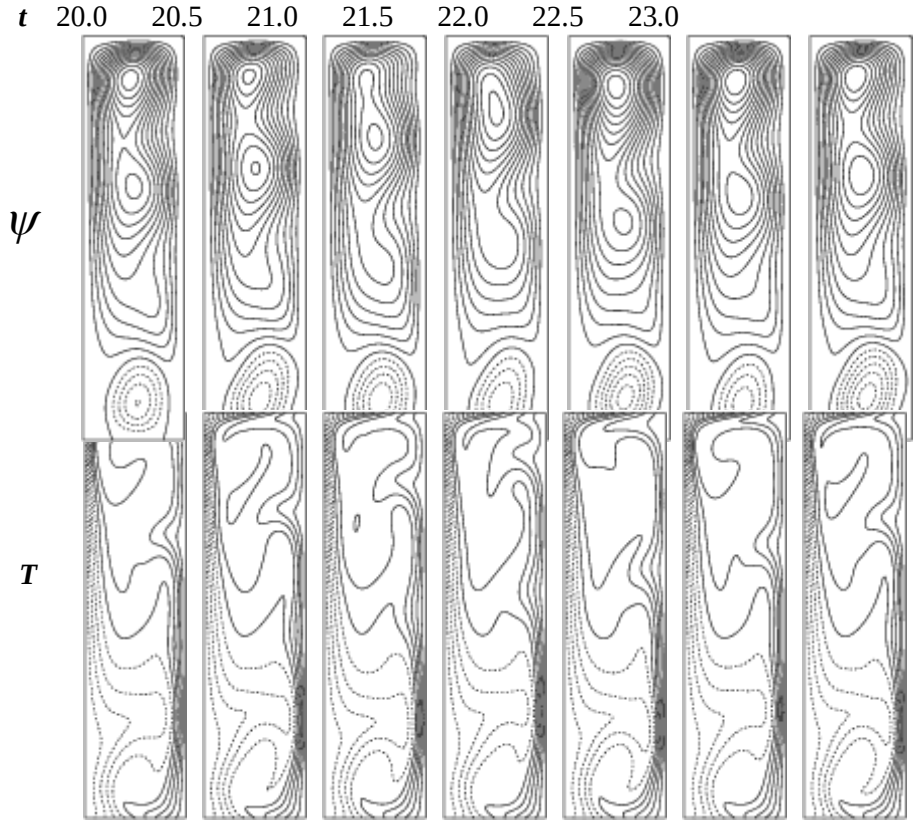

Figure 9: Secondary flow patterns and temperature distributions for *Dn* = 100, *Gr* = 500 for the aspect ratio *l* = 4 at time $20.0 \le t \le 23.0$ **.**

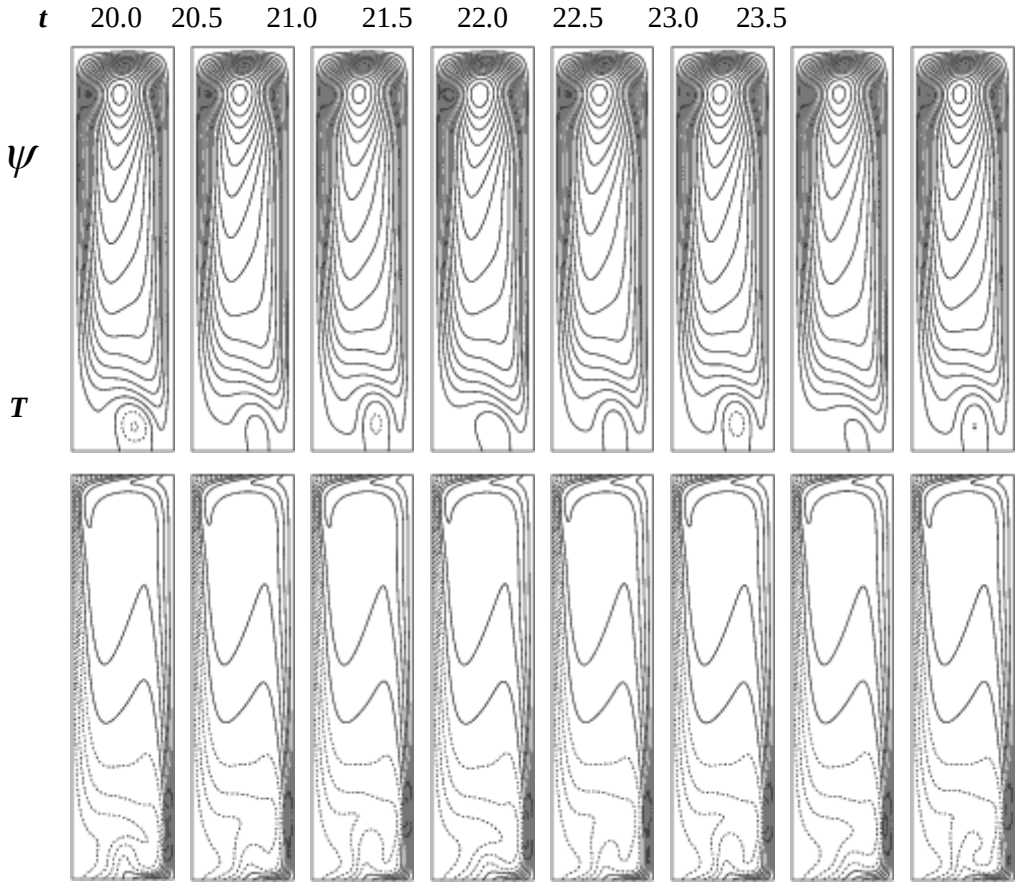

Figure 10: Secondary flow patterns and temperature distributions for *Dn* = 100, *Gr* = 1000 for the aspect ratio *l* = 4 at time $20.0 \le t \le 23.5$**.**

Then we perform time-evolution of λ for *Dn* = 100 and *Gr* = 100, 500 and 1000 for the aspect ratio *l* = 4, as shown in Fig. 8(a). It is found that the unsteady flow is a steady-state solution for *Gr* = 100 but a periodic solution at *Gr* = 500 and a multi-periodic solution at *Gr* = 1000. Since the flow is a steady-state solution for *Gr* =100, *Dn* = 100 and *l* = 4, we show a single contour of secondary flow pattern and the temperature profile at time *t* = 20 in Fig. 8(b). It is also found that the steady-state solution is an asymmetric two-vortex solution. In order to see the periodic change of the flow patterns and temperature distributions, as time proceeds, typical contours of secondary flow patterns and temperature profiles for *Dn* = 100 and *Gr* = 500 at *l* = 4 are shown in Fig. 9 for $20.0 \le t \le 23.0$. As seen in Fig. 9, the periodic oscillation at *Gr* = 500 is an asymmetric two-vortex solution. The upper vortex is a large vortex comprising with two minor vortices. Then we show typical contours of secondary flow patterns and temperature distributions for the multi-periodic oscillation at *Dn* = 100, *Gr* = 1000 for the aspect ratio *l* = 4 in Fig. 10 for the time interval $20.0 \le t \le 23.5$, where it is seen that the unsteady flow at *Gr* = 1000 oscillates periodically between the asymmetric two-vortex solutions with one large vortex dominating the smaller one. It is found that as the Grashof number increases the symmetry with respect to $y = 0$ gradually disappears and a large vortex covers the whole cross-section of the duct. It is also found that the oscillation tends to occur when the Grashof number or the aspect ratio is increased, if the Dean number is kept constant.

Conclusions

We obtained unsteady solutions for the non-thermal flows through a curved rectangular duct of aspect ratios 1 to 4 for the Dean number *Dn* = 100 with a temperature difference between the vertical sidewalls for the Grashof number *Gr* = 100, 500 and 1000. The outer wall of the duct is heated while the inner wall cooled. Spectral method is used as a basic tool to solve the system of non-linear differential equations.

We studied the unsteady solutions of the velocity and temperature fields and it is found that the larger *Gr* is, the flow loses its symmetry with respect to the plane $y = 0$. For some cases, on the other hand, the symmetry is approximately maintained when *Dn* is increased. Therefore the temperature difference and the pressure gradient along the duct affect the fluid in an opposite manner as for the symmetry of the flow. It is also found that the flow becomes time-dependent and periodic when *Dn* or *Gr* is increased. For this case, the two effects, centrifugal effect and buoyancy effect, affect the fluid in a similar manner. For large aspect ratios, it is found that, the transition from periodic to chaotic state occurs if the Dean number or the Grashof number is small.

REFERENCES

Berger, S. A.; Talbot, L. and Yao, L. S (1983). Flow in curved pipes. *Annual Review of Fluid Mechanics,* **35**, 461–512.

Chandratilleke, T. T. and Nursubyakto (2003). Numerical prediction of secondary flow and convective heat transfer in externally heated curved rectangular ducts. *International Journal of Thermal Sciences*, **42** 187-198.

Dean, W. R (1927). Note on the motion of fluid in a curved pipe. *Philosophical Magazine,* **4**, 208–223.

Dennis, S. C. R. and Ng, M (1982). Dual solutions for steady laminar flow through a curved tube. *Quarterly Journal of Mechanics and Applied Mathematics,* **35**, 305-324.

Ito, H (1987). Flow in curved pipes. *JSME International Journal*, **30**, 543–552.

Mondal, R. N (2006). Isothermal and non-isothermal flows through curved ducts with square and rectangular cross sections, Ph.D. Thesis, Department of Mechanical Engineering, Okayama University, Japan.

Mondal, R. N.; Kaga, Y.; Hyakutake, T. and Yanase, S (2006). Effects of curvature and convective heat transfer in curved square duct flows. *Trans. ASME, Journal of Fluids Engineering*, **128**(9), 1013–1023.

Mondal, R. N. Datta, A. K., Roy, B. and Mondal, B (2010). Numerical prediction of secondary flow and unsteady solutions through a curved rectangular duct, *Int. J. Appl. Sci. & Comp*, **17(**1), pp. 37-49**.**

Nandakumar K. and Masliyah, H. J (1982). Bifurcation in steady laminar flow through curved tubes. *Journal of Fluid Mechanics*, **119**, 475-490.

Nandakumar, K. and Masliyah, J. H (1986). Swirling flow and heat transfer in coiled and twisted pipes. *Advanced Transport Process*, **4**, 49–112.

Wang, L. and Yang, T (2004). Bifurcation and stability of forced convection in curved ducts of square cross section. *International Journal of Heat and Mass Transfer*, **47**, 2971-2987.

Winters, K. H (1987). A bifurcation study of laminar flow in a curved tube of rectangular cross-section. *Journal of Fluid Mechanics*, **180**, 343–369

Yanase, S. and Nishiyama, K (1998). On the bifurcation of laminar flows through a curved rectangular tube. *Journal of the Physical Society of Japan***, 57,** 3790-3795.

Yanase, S.; Mondal, R. N.; Kaga, Y. and Yamamoto, K (2005a). Transition from steady to chaotic states of isothermal and non-isothermal flows through a curved rectangular duct. *Journal of the Physical Society of Japan*, **74**(1), 345–358.

Yanase, S.; Mondal, R. N. and Kaga, Y (2005b). Numerical study of non-isothermal flow with convective heat transfer in a curved rectangular duct. *International Journal of Thermal Sci*ences, **44**(11), 1047–1060.

Yang, Z. and Keller, H. B (1986). Multiple laminar flows through curved pipes. *Applied Numerical Mathematics*, **2**, 257-271.